Joint Diseases and Related Surgery

Jt Dis Relat Surg
2025;36(3):648-658

ORIGINAL ARTICLE

Effect of fracture level on optimal Kirschner wire configuration in pediatric supracondylar humerus fractures: A finite element analysis

Turkay Yilmaz, MD[1], Ismail Hakki Dur[2], Tugce Kabakci[2], Muhammed Abdulkadir Bulut, MD[3], Bengu Akgok[2], Ulas Can Kolac, MD[3], Mustafa Ozkaya, MD[4], Sancar Bakircioglu, MD[5]

[1]Department of Orthopedics and Traumatology, Alaca State Hospital, Çorum, Türkiye
[2]TOBB University of Economy and Technology, Faculty of Medicine, Ankara, Türkiye
[3]Department of Orthopedics and Traumatology, Hacettepe University Faculty of Medicine, Ankara, Türkiye
[4]Department of Mechanical Engineering, KTO Karatay University, Konya, Türkiye
[5]Department of Orthopedics and Traumatology, TOBB University of Economy and Technology, Ankara, Türkiye

ABSTRACT

Objectives: This study aims to evaluate the biomechanical stability of three pin configurations for transverse supracondylar humerus fractures at various levels using finite element analysis (FEA).

Materials and methods: Computed tomography data from a six-year-old child were used to generate a humerus bone model. Four different fracture levels (low, transolecranon, high, and ultrahigh) and three pin fixation techniques (one lateral and one medial cross-pin [1-1M], two lateral capitellar pins [1-1C], and three lateral capitellar pins [2-1C]) were designed for the study. Translational stiffness and rotational stiffness in all directions were analyzed in the mesh models. Convergence data and stiffness data were obtained in the FEA.

Results: The translational and rotational stiffness values varied across fracture levels and pin configurations. Under valgus loading, the 1-1M configuration provided the highest stability in ultrahigh fractures (3289 N/mm), while the 2-1C configuration showed superior valgus and varus stability in low and transolecranon fractures. During extension and flexion loading, the 1-1M configuration yielded the highest stiffness values for transolecranon and high fractures, while the 2-1C configuration demonstrated increased stability in low and ultrahigh fractures. For rotational loading, 1-1M produced the highest inward and outward stiffness values in low-level fractures (9175 and 11035 N·mm/degree, respectively), whereas 2-1C displayed greater rotational stiffness in ultrahigh fractures.

Conclusion: This preliminary study suggests that no single pin configuration is ideal for all fracture types, and the choice should be based on the specific fracture case.

Keywords: Biomechanics, finite element, fracture level, fracture type, Kirschner-wire, pediatric elbow fractures, pin configuration, supracondylar humerus fractures.

Supracondylar fractures account for 15% of pediatric fractures and are most commonly seen in children aged five to seven years.[1,2] The majority of these fractures are extension-type fractures (97 to 98%) caused by falls onto an outstretched hand.[3,4] In the treatment of displaced supracondylar fractures, the main strategy is closed reduction and pinning with Kirschner wires (K-wires), but debates are still ongoing regarding the use of only lateral pins versus both medial and lateral cross-pin configurations.[5-7] Cross-pin configurations are proposed to increase rotational stability compared

Received: March 05, 2025
Accepted: May 19, 2025
Published online: July 21, 2025

Correspondence: Sancar Bakircioglu, MD. TOBB ETÜ Ekonomi ve Teknoloji Üniversitesi, Ortopedi ve Travmatoloji Anabilim Dalı, 06510 Çankaya, Ankara, Türkiye.

E-mail: bakircioglusancar@gmail.com

Doi: 10.52312/jdrs.2025.2248

Citation: Yilmaz T, Dur IH, Kabakci T, Bulut MA, Akgok B, Kolac UC, et al. Effect of fracture level on optimal Kirschner wire configuration in pediatric supracondylar humerus fractures: A finite element analysis. Jt Dis Relat Surg 2025;36(3):648-658. doi: 10.52312/jdrs.2025.2248.

to lateral pin configurations.[8,9] However, the use of medial pinning has significant disadvantages, including a three-fold increased risk of iatrogenic ulnar nerve injury and potential aesthetic issues due to the incision made for medial pinning.[10]

Various biomechanical studies have investigated the effect of different pin configurations on stability across multiple scenarios.[11-14] In recent years, the impact of fracture type such as obliquity and fracture level on postoperative outcomes for supracondylar fractures has been investigated; however, in studies utilizing finite element analysis (FEA), the effect of pin configurations on stiffness at different fracture levels has not been investigated.[15-19] Identifying the optimal pin configuration according to the fracture level could significantly contribute to daily practice in the management of pediatric supracondylar fractures.

In the present study, we aimed to evaluate the stiffness in flexion, extension, varus, valgus, internal rotation, and external rotation of three pin configurations, applied using the ideal techniques described in the literature,[17,20,21] in scenarios of transverse supracondylar humerus fractures at different fracture levels.

MATERIALS AND METHODS

The study was conducted between January 2025 and March 2025. The mechanics of different pinning configurations in the fixation of transverse supracondylar humerus fractures were investigated in child's humerus using the FEA. The generation of the bone model, fracture locations, pinning configurations, and the settings of the FEA are explained in detail below. This study did not require ethical approval as it was based on previously obtained and anonymized computed tomography (CT) data, and no human or animal intervention was performed.

The generation of the bone model

The distal humerus used in this study includes the cortical and cancellous bone, ossific nucleus, and cartilage (Figure 1a). Computed tomography data of a six-year-old male child were used to generate the humerus bone model. This CT was taken in emergency service for a soft tissue trauma to exclude a bone fracture. The radiology CT report confirmed no signs of a fracture and indicated normal bone structure and alignment. Scanning was performed using a Siemens SOMATOM Force CT scanner (Model ID: 792CT75819, Serial No: 75819; Siemens Healthineers, Forchheim, Germany), as confirmed by institutional service records. The imaging parameters were as follows: slice thickness: 1.0 mm, slice interval: 0.5 mm, tube voltage: 120 kV, tube current: 200 mA, bone window settings; width 1,500 HU, level 300 HU. These settings provided sufficient image quality for three-dimensional (3D) segmentation of cortical and cancellous bone, ossific nucleus, and cartilage structures, allowing FEA reconstruction.

The DiCOM images were taken from the CT in JPEG format and inserted into SolidWorks (Dassault Systems SolidWorks Corp., Waltham, MA, USA), which is a 3D CAD modeling software. The JPEG images were arranged layer by layer from proximal to distal in SolidWorks just as in the CT. Inner and outer borders of the cortical bone were drawn in each layer. By using the "loft" command, a solid body was generated with the guidance of the outer borders in each layer. Another solid body intersecting with the first body was also generated with the guidance of the inner borders, using the same approach. Then, the latter one was subtracted from the former one, which eventually resulted in two separate bodies representing the cortical and trabecular bones. The ossific nucleus was also generated by using the cortical borders. The cartilage was modeled appropriately, encasing the bones and ossific nucleus, again with the help of the CT data. Written informed consent was obtained from the parents of the patient for the use of imaging data for academic and research purposes.

Fracture locations and pinning configurations

Following the generation of the humerus model, fractures and pinning configurations were created in SpaceClaim (Ansys Inc., Canonsburg, PA, USA), which is another 3D CAD modeling software. Four fracture types at different levels were generated on the humerus, designated as low, transolecranon, high, and ultrahigh (Figure 1b). The classification of fracture levels was adapted from the criteria described by Kang et al.[16] To determine the level of fracture, a reference line was defined:

On the sagittal plane, at the isthmus of the distal humerus, and on the anteroposterior (AP) plane, as a line connecting the medial epicondyle, the olecranon fossa, and the lateral epicondyle.

- High fractures were defined as those located entirely above this reference line.
- Low fractures were defined as those involving or below the line.

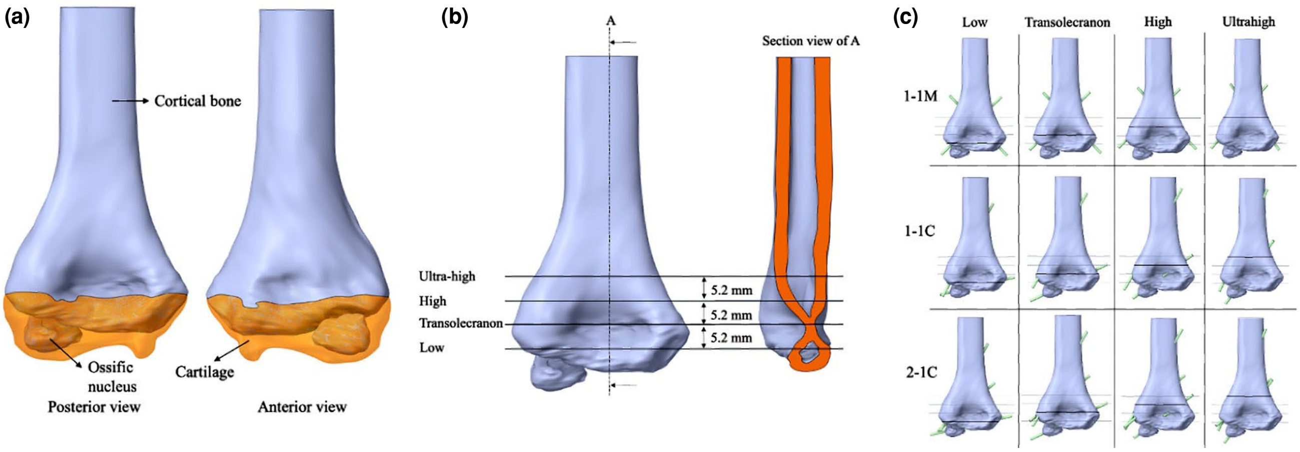

FIGURE 1. (a) The CAD model of the distal humerus and **(b)** the locations of the four fractures. **(c)** The fracture locations and pinning configurations.
CAD: Computer-aided design.

- Transolecranon fractures were those traversing the midpoint of the olecranon fossa.
- Ultrahigh fractures were defined as those more than 15 mm proximal to the reference line, approaching the metaphyseal-diaphyseal junction.

These fractures were fixed with various lateral capitellar and cross-pinning configurations using 1.6 mm K-wires (Figure 1c). Additionally, the lateral capitellar pinning has two configurations: one performed with two wires and the other with three. Thus, each of the four fractures had three pinning configurations, resulting in a total of 12 models. For lateral pinning groups, all proximal pins were placed parallel to the lateral metaphyseal flare as described by Hamdi et al.[22] For the entry point, proximal pins were placed posterolateral to the ossific nucleus of the capitellum (ONC) for maximum divergence, as described by Ji et al.[20] and Wang et al.[21] Ji et al.[20] also found that in the eight zones of the distal humerus, lateral pinning mainly exited between the –2 zone and the +1 zone (94.4%).[20] Therefore, to achieve maximum divergence, the +1 zone was targeted as the exit zone for proximal pins. Cross pins were placed from the middle of the medial epicondyle and at the same level on the lateral side, as described by Kamara et al.[17] The pinning trajectory and exit points for distal capitellar pins were altered accordingly for fractures. For lateral pins, each pin was aimed to intersect with the lateral $^{1}/_{3}$ part of the fracture line to achieve maximum divergence. In contrast, for cross pins, each pin was aimed to intersect with the medial $^{1}/_{3}$ part of the fracture line to achieve the maximum distance to the fracture apex. For the sagittal plane, a divergent sagittal pin configuration described by Pothong et al.[23] was used for all possible pin configurations, with the exception being the distal pins of the capitellar group, which pass directly through the middle of the ONC to achieve maximum stability according to Kamara et al.[17]

Finite element analysis

The FEAs were carried out in ANSYS Workbench (Ansys Inc., Canonsburg, PA, USA). The material properties for the cortical bone of a six-year-old child, cancellous bone, ossific nucleus, cartilage, and pins are provided in Table I.[17,24,25] The 316L stainless steel was used for the pins. It was assumed that all materials exhibited linear elastic and isotropic material behavior under loading.

TABLE I
Material properties of the cortical and cancellous bones, ossific nucleus, cartilage, and pins, including MPa and poisson's ratio

	MPa	Poisson's ratio
Cortical bone	11670	0.28
Cancellous bone	70	0.2
Ossific nucleus	70	0.2
Cartilage	15	0.45
K-wires (316L SS)	200000	0.33

MPa: Modulus of elasticity.

Appropriate contact conditions were defined to maintain numerical accuracy and achieve convergence of the simulation. Bonded contact was assigned between the cortical and cancellous bones, resulting in an inseparable connection. At the interface between the pins and cortical bone, bonded contact was also used, as the cortical bone tightly holds the pins, and slipping of the pin from the bone is generally not possible under physiological loading. On the other hand, at the interfaces between the pins and cancellous bone and between the pins and ossific nucleus, sliding was allowed by using frictional contact, as the cancellous bone and ossific nucleus are not as stiff as cortical bone and can be deformed by the pins under physiological loading, allowing for a small amount of sliding. This sliding is particularly likely around the fracture level. At the interfaces between the pins and the cancellous bone, as well as between the pins and the ossific nucleus, a frictional contact with a static coefficient of 0.3 was applied.[26] The contacts between the bone segments above and below the fracture line were assigned as frictional with a static friction coefficient of 0.46.[27]

The mesh model is crucial in FEA simulations, as two different mesh models of the same structure can cause significant differences in numerical results. In the present study, second-order tetrahedral and hexahedral elements were used. In the meshing procedure, a finer mesh model provides more accurate results and converges better to experimental data compared to a coarser mesh model. To improve the mesh model, continuously increasing the number of elements beyond a certain limit does not change the results; on the contrary, it increases the computational load and processing time. Therefore, convergence analysis was performed in this study to determine the ideal number of elements. In the convergence analysis, if the difference between the strain energies (mJ) obtained from the subsequent three analyses was less than 1%, the results were considered converged. The mesh model for a distal humerus and pinning configuration can be seen in Figure 2.

Setting the boundary and loading conditions is a critical step in correctly mimicking physiological conditions. In the present study, the upper end of the model distal humerus was fixed in all degrees of freedom, and its displacement was restricted. The loading was applied through two circular loading surfaces created on the cartilage (Figure 3a). The reason for using two circular areas for loading is to ensure that the load is distributed over a larger area on the joint surface, similar to physiological loading. While this approach does not directly model soft tissue attachments (e.g., the biceps brachii tendon or collateral ligaments), it allows for standardized and reproducible force application in line with previous

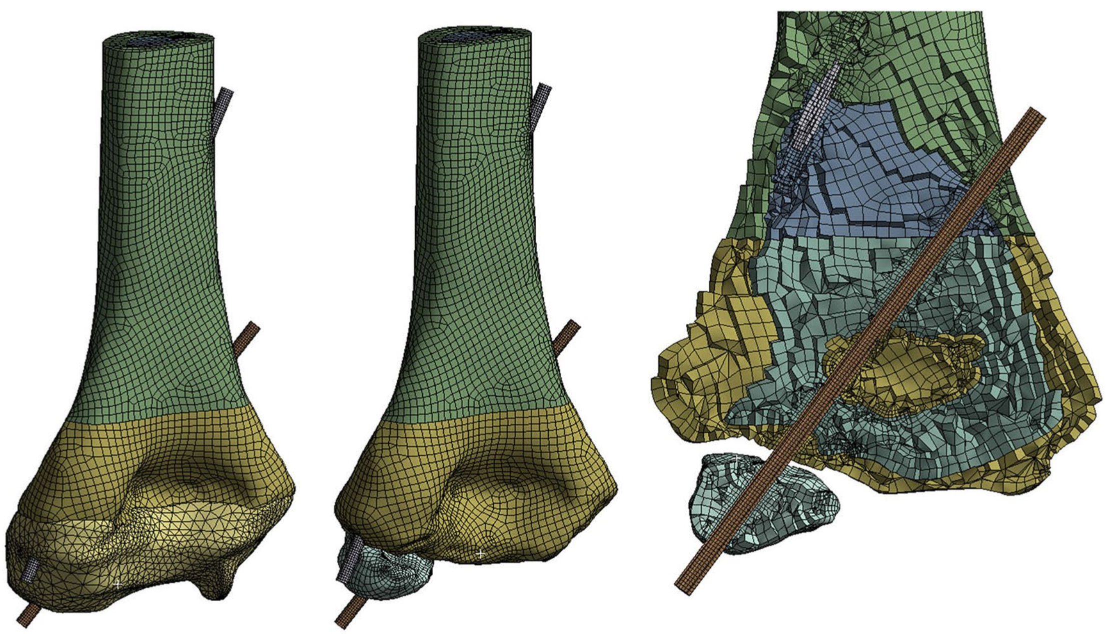

FIGURE 2 The mesh model of a distal humerus and pinning configuration. The whole model is shown on the left, the model without cartilage in the middle, and a cross-section of the model on the right.

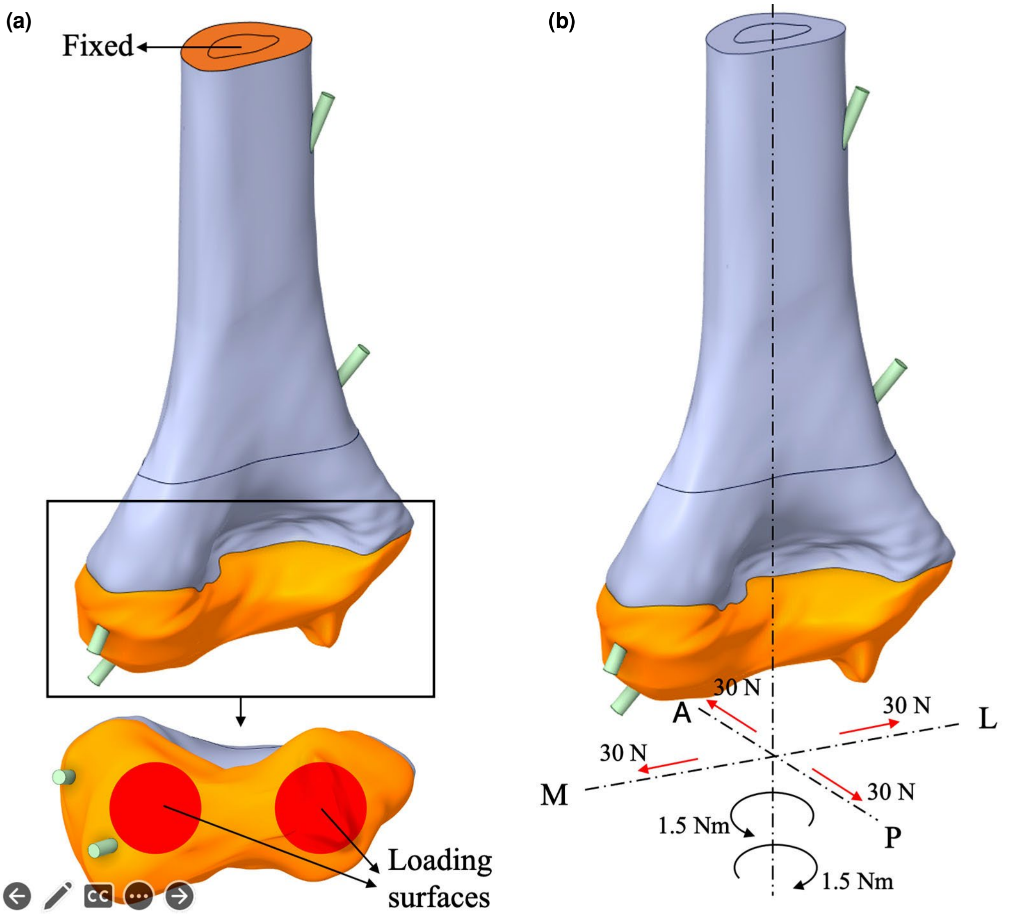

FIGURE 3. **(a)** The boundary conditions and, **(b)** the loading conditions.

FEA studies.[17,28] Six loading conditions-four translations with a 30 N load in the medial, lateral, anterior, and posterior directions, and two rotations with 1.5 Nm of torque in the inward and outward directions-were carried out separately in this study (Figure 3b). There were six loading conditions for each of the 12 pin configurations; therefore, 72 different analyses were conducted in total.

Interpretation of the results

The translational stiffness and rotational stiffness were used to compare the mechanical behaviors of the pinning configurations. The translational stiffness (N/mm) was calculated as the ratio of the applied load to the displacement of the distal bone fragment in the loading direction. The rotational stiffness (N.mm/degree) was calculated as the ratio of the applied torque to the angular displacement of the distal bone fragment in the torque direction.

RESULTS

Results of the convergence analysis

The result of the convergence analysis is shown in Figure 4. This figure illustrates the curve of total strain energies changing with respect to different numbers of elements. It also shows the percentage errors (e) in the total strain energies between the different numbers of elements. As can be seen, the percentage error decreased with increasing numbers of elements, and the subsequent errors between the models with 109,476 and 124,821 elements, as well as between the models with 124,821 and 132,596 elements, were below the 1% limit. Therefore, it can be said that the model converged with 109,476 elements. However, the mesh settings for the model with 124,821 elements were used in all subsequent analyses to guarantee the accuracy of results for the analyses of all pinning configurations. The element sizes in the converged model are 1 mm for the cortical bone,

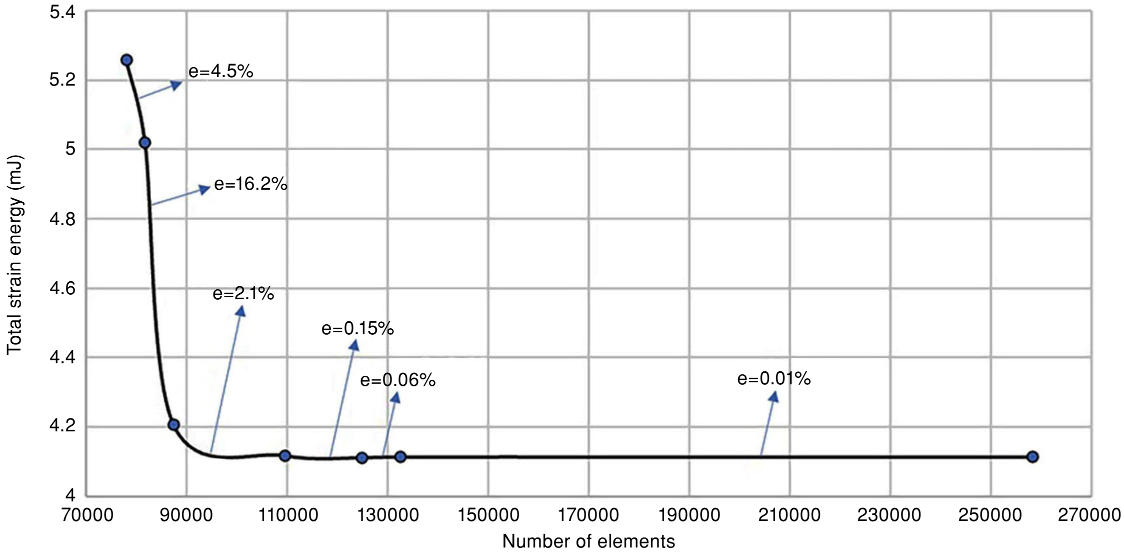

FIGURE 4. Results of the convergence analysis, showing the relationship between the number of elements and total strain energy.

cancellous bone, and ossific nucleus, and 0.3 mm for the pins and the bone-pin interface.

Results of stiffness under loading conditions

The translational and rotational stiffness values for each pin configuration at varying fracture levels under specific loading conditions are presented in Table II and Figure 5.

Under valgus loading, the 1-1M configuration demonstrated the highest stability in ultrahigh fractures (3289 N/mm), outperforming the 2-1C and 1-1C configurations. For low and transolecranon fractures, the 2-1C configuration provided the greatest valgus and varus stability.

In extension loading, the 1-1M configuration yielded the highest stiffness for transolecranon and high fractures (up to 8530 N/mm), while 2-1C performed best for low and ultrahigh fractures (5455 N/mm and 6522 N/mm, respectively).

TABLE II

Translational and rotational stiffness (N/mm and N·mm/°) for different pin configurations (1-1M, 1-1C, 2-1C) across four fracture levels (low, transolecranon, high, and ultrahigh) under various loading conditions

	Configuration	Varus/medial (N/mm)	Valgus/lateral (N/mm)	Entension/posterior (N/mm)	Flexion/anterior (N/mm)	Inward rotation (N*mm/°)	Outward rotation (N*mm/°)
	1-1M	4854	13274	4491	2295	9175	11035
Low	1-1C	6287	9317	853	2595	5594	3767
	2-1C	7614	15228	1115	3311	5770	4121
	1-1M	3851	2660	1765	5300	2564	2498
Transcolecranon	1-1C	14181	7143	2320	3236	12817	8104
	2-1C	23899	8850	2676	4021	13870	8684
	1-1M	3135	2522	3521	8065	2151	1877
High	1-1C	8475	3209	2410	3534	9706	8629
	2-1C	19501	6843	3394	5455	11130	9391
	1-1M	3836	3289	3722	5515	392	754
Ultrahigh	1-1C	7198	859	726	2492	1216	887
	2-1C	15997	2197	1375	6522	1270	1107

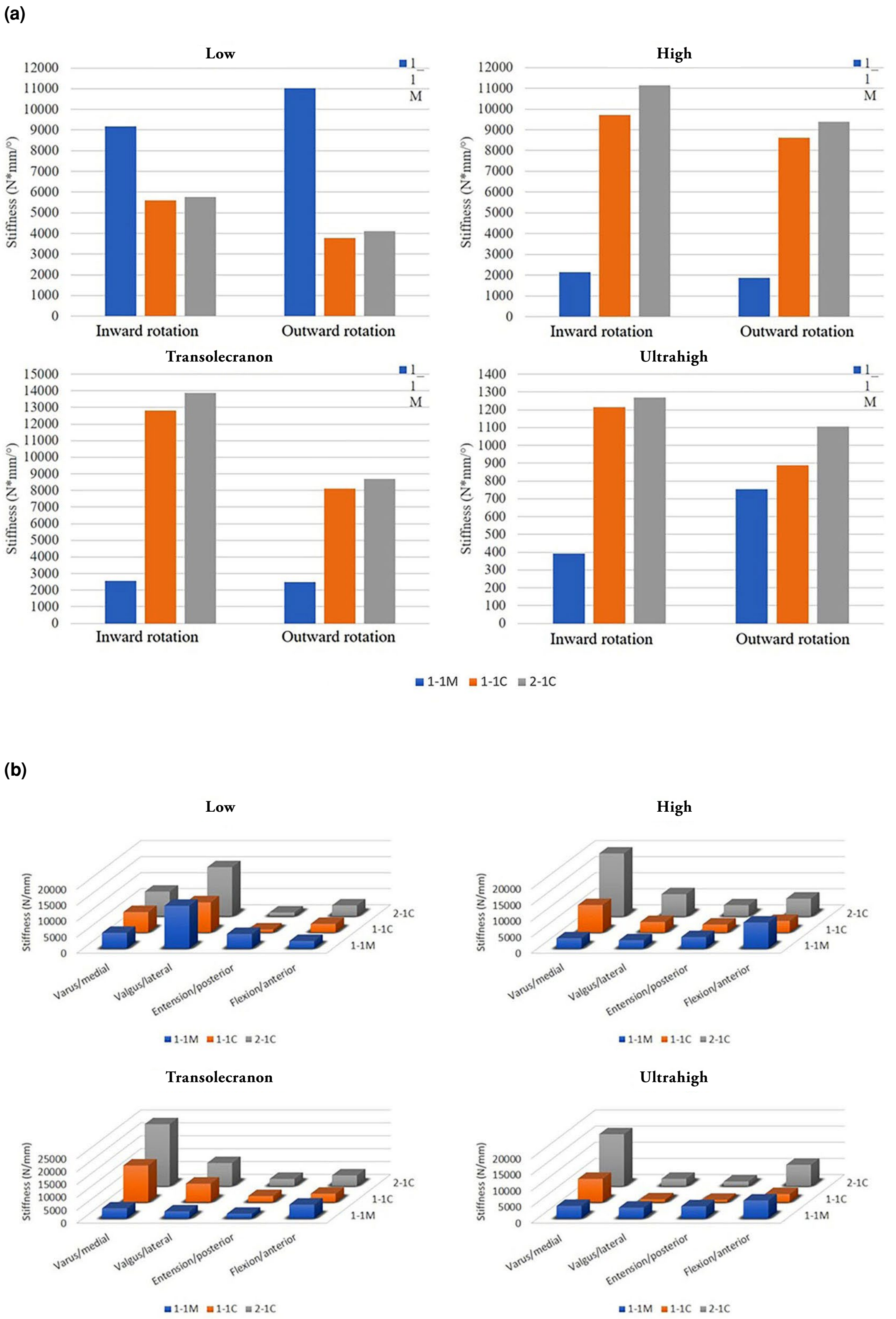

FIGURE 5. (a) Rotational stiffness (N·mm/degree) in inward and outward rotation for different pin configurations (1-1M, 1-1C, 2-1C) across four fracture levels (Low, High, Transolecranon, and Ultrahigh). **(b)** Translational stiffness (N/mm) in different loading directions (varus/medial, valgus/lateral, extension/posterior, flexion/anterior) for various pin configurations (1-1M, 1-1C, 2-1C) across four fracture levels.

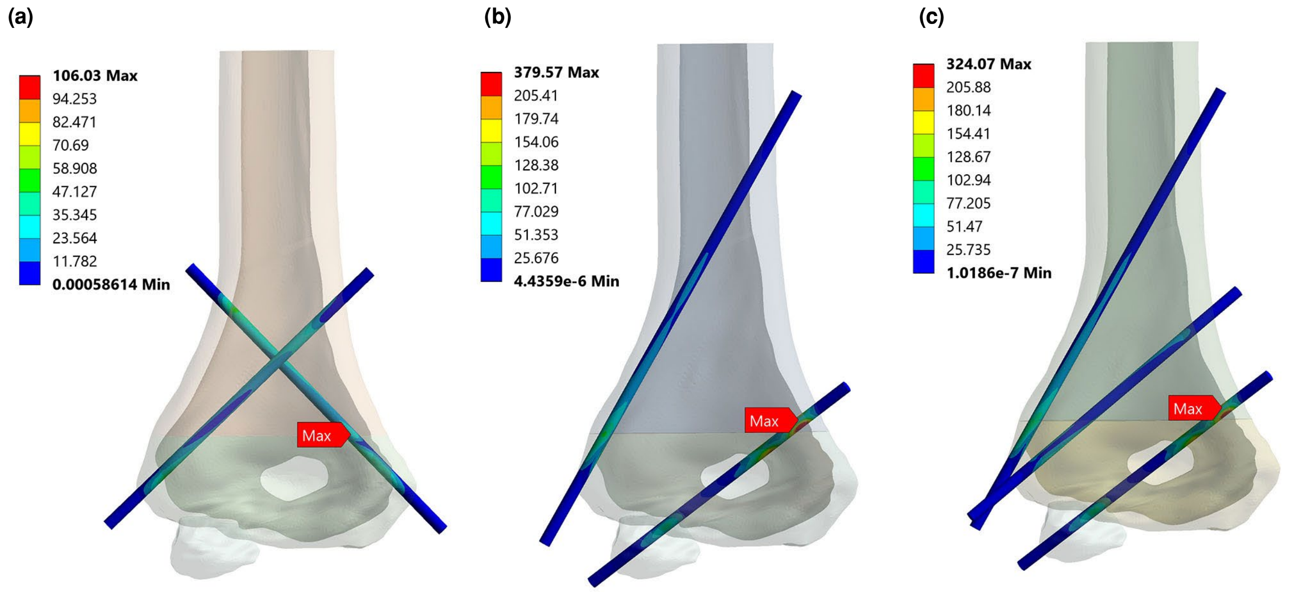

FIGURE 6. Von Mises stress distribution on K-wires for **(a)** 1-1M, **(b)** 1-1C, and **(c)** 2-1C configurations under posterior extension loading in a high-level transverse supracondylar humerus fracture. Warmer colors indicate higher stress concentrations, particularly around pin entry points and along the fracture interface.

During flexion loading, the 1-1M configuration showed superior stability in transolecranon and high fractures (5300-8065 N/mm), whereas 2-1C offered the highest resistance in low and ultrahigh fractures.

For rotational loading, the 1-1M configuration delivered the highest inward and outward rotational stiffness in low-level fractures (9175 N·mm/degree and 11035 N·mm/degree, respectively). In contrast, in ultrahigh fractures, the 2-1C configuration provided greater rotational stability than both 1-1C and 1-1M. To support the stiffness results with a visual representation, von Mises stress contour plots were generated for the 1-1M, 1-1C, and 2-1C configurations under posterior extension loading in high-level fractures (Figure 6). These plots highlight areas of stress concentration on the K-wires, particularly around the pin entry points and fracture interface, reinforcing the mechanical interpretation of the fixation stability. The 1-1M configuration appeared less prone to failure due to lower stress values under several loading conditions, while rotational forces consistently produced the highest stress across all fracture types and fixation methods.

DISCUSSION

Our study is the first to investigate the fixation stability of different pin configurations placed ideally according to various fracture heights in supracondylar fractures using FEA. The primary finding of this study is that there is no single ideal option for different fracture scenarios and that different configurations should be evaluated based on the type of fracture.

In low fractures, the 1-1M configuration proves to be a logical choice for extension-direction unstable fractures, given its highest stiffness against rotational forces and distinctively high stiffness for extension force compared to other configurations. For transolecranon fractures, considering the potential ulnar nerve injury, it might be prudent to avoid the 1-1M configuration due to its low stiffness in varus-valgus and internal and external rotational forces. Due to its low stiffness against rotational and varus-valgus forces in high fractures, the 1-1M configuration has been found to be less than ideal. The most optimal option for high fractures is the 2-1C configuration. However, the 1-1C configuration also provides similar results to 2-1C under rotational and flexion-extension forces in high fractures. Therefore, this configuration may be used for fractures with a low probability of varus-valgus translation to reduce anesthesia time, radiation exposure, and potential physeal damage.[29] In ultrahigh fractures, the 1-1M configuration fails to provide sufficient stability against rotational forces, and the 1-1C configuration is inadequate against extension-flexion and valgus forces. Considering the instability of such fractures, the 2-1C configuration may be the most prudent choice.[16,28] In light of these findings, as the fracture level becomes more proximal, it may be advisable to move away from the 1-1M configuration to avoid potential ulnar nerve damage. With a comprehensive evaluation that considers the unique nature of each fracture, the 1-1C configuration could be recommended. However, in cases where sufficient rigidity is a concern, the use of the 2-1C configuration should not be disregarded.

Kamara et al.'s study,[17] which evaluated the stiffness of different configurations in extension-type fractures originating from the transolecranon region using FEA, observed that the 2-lateral, 1-medial pin configuration provided the highest stability in all directions. In these fractures, the configuration with a third pin passing through the olecranon fossa showed increased stiffness in flexion and extension, while the configuration with the third pin passing laterally showed increased stability in varus and valgus compared to the 2-pin configuration. In our study, however, there was no significant difference in stability, except for varus, between the 1-1C and 2-1C configurations in transolecranon fractures. One key reason for this discrepancy is that Kamara et al.'s study[17] investigated a single transverse fracture level at the olecranon fossa, whereas our study analyzed four distinct fracture levels. We found that the relative stability of each pin configuration varied significantly depending on the vertical location of the fracture, especially in ultrahigh and low-level fractures.

Additionally, differences in mesh construction, boundary conditions, and pin modeling strategies may have contributed to variation in stiffness values. Kamara et al.[17] also evaluated more diverse 3-pin arrangements, while our study focused on consistent 2- and 3-pin patterns across multiple heights. Despite these methodological differences, both studies demonstrate the importance of pin trajectory and pin number in achieving optimal fixation stability.

In a study by Liu et al.[28] which conducted a FEA on metaphyseal-diaphyseal junction fractures, a configuration with two lateral and one medial K-wire provided the best stability against rotational, flexion, and varus forces, while a configuration with three divergent lateral K-wires offered the best stability against extension and valgus forces. In our study, the 2-1C configuration demonstrated higher stiffness values than the 1-1M configuration against varus, flexion, and rotational forces, but was less stiff than the 1-1M configuration in extension and valgus forces. The hypothesis that loss of reduction following lateral pinning begins with rotation, and the fact that fractures with internal rotation are particularly more unstable, suggest that the role of medial pinning in such fractures should be reconsidered by the surgeon.[13,30]

A recent FEA study by Bozoğlan et al.[19] compared multiple fixation methods across transverse and oblique high supracondylar fractures in a pediatric model, highlighting that optimal pin configurations vary significantly by fracture morphology and loading direction. Their findings further emphasize the importance of individualized fixation strategies, consistent with the conclusions of our study.

One of the main limitations to this study is the exclusive creation of transverse fractures in the models, thereby excluding the assessment of oblique or comminuted fractures. The pin configurations investigated in the study are considered ideal according to the literature. Future studies should aim to incorporate dynamic loading conditions and simulate soft tissue forces, such as those exerted by the biceps brachii and collateral ligaments, to more accurately represent physiological biomechanics. Additionally, evaluating oblique, comminuted, and flexion-type supracondylar fractures, as well as the effects of imperfect pin placement, would enhance the clinical applicability of FEA models. Validation with cadaveric or *in vivo* biomechanical data is also warranted to strengthen the translational value of simulation findings.

In conclusion, these results highlight the importance of evaluating each supracondylar fracture individually, both pre- and intraoperatively, with consideration of fracture level. Our findings suggest that low-level fractures may benefit from cross-pinning for improved stability, whereas ultrahigh fractures are more successfully managed with three lateral pins to minimize the risk of ulnar nerve injury. These results offer orthopedic surgeons valuable guidance on selecting additional lateral or medial pinning strategies according to fracture height.

Data Sharing Statement: The data that support the findings of this study are available from the corresponding author upon reasonable request.

Author Contributions: Data collection and analysis were performed: T.Y., M.A.B., M.O.; The first draft of the manuscript was written: T.Y., I.H.D., T.K.; The manuscript was reviewed and edited prior to submission: B.A., S.B., U.C.K. All authors contributed to the study conception and design.

Conflict of Interest: The authors declared no conflicts of interest with respect to the authorship and/or publication of this article.

Funding: The authors received no financial support for the research and/or authorship of this article.

REFERENCES

1. Gültekin MZ, Doğar F, Sarı AS, Coşkun F, Yıldırım A. The role of the psychological attributes of parents and children, and fracture history in upper extremity fractures in school-age and adolescents: A case-control study. Jt Dis Relat Surg 2024;35:315-23. doi: 10.52312/jdrs.2023.1486.
2. Barr LV. Paediatric supracondylar humeral fractures: Epidemiology, mechanisms and incidence during school holidays. J Child Orthop 2014;8:167-70. doi: 10.1007/s11832-014-0577-0.
3. Steinman S, Bastrom TP, Newton PO, Mubarak SJ. Beware of ulnar nerve entrapment in flexion-type supracondylar humerus fractures. J Child Orthop 2007;1:177-80. doi: 10.1007/s11832-007-0034-4.
4. Delniotis I, Dionellis P, Gekas CC, Arapoglou D, Tsantekidis D, Goulios V, et al. Flexion-type supracondylar humeral fracture with ulnar nerve injury in children: Two case reports and review of the literature. Am J Case Rep 2020;21:e921293. doi: 10.12659/AJCR.921293.
5. Reisoglu A, Kazimoglu C, Hanay E, Agus H. Is pin configuration the only factor causing loss of reduction in the management of pediatric type III supracondylar fractures? Acta Orthop Traumatol Turc 2017;51:34-8. doi: 10.1016/j.aott.2016.11.003.
6. Gaston RG, Cates TB, Devito D, Schmitz M, Schrader T, Busch M, et al. Medial and lateral pin versus lateral-entry pin fixation for Type 3 supracondylar fractures in children: A prospective, surgeon-randomized study. J Pediatr Orthop 2010;30:799-806. doi: 10.1097/BPO.0b013e3181f73d59.
7. Zhao JG, Wang J, Zhang P. Is lateral pin fixation for displaced supracondylar fractures of the humerus better than crossed pins in children? Clin Orthop Relat Res 2013;471:2942-53. doi: 10.1007/s11999-013-3025-4.
8. Brauer CA, Lee BM, Bae DS, Waters PM, Kocher MS. A systematic review of medial and lateral entry pinning versus lateral entry pinning for supracondylar fractures of the humerus. J Pediatr Orthop 2007;27:181-6. doi: 10.1097/bpo.0b013e3180316cf1.
9. Larson L, Firoozbakhsh K, Passarelli R, Bosch P. Biomechanical analysis of pinning techniques for pediatric supracondylar humerus fractures. J Pediatr Orthop 2006;26:573-8. doi: 10.1097/01.bpo.0000230336.26652.1c.
10. Dekker AE, Krijnen P, Schipper IB. Results of crossed versus lateral entry K-wire fixation of displaced pediatric supracondylar humeral fractures: A systematic review and meta-analysis. Injury 2016;47:2391-8. doi: 10.1016/j.injury.2016.08.022.
11. Lee SS, Mahar AT, Miesen D, Newton PO. Displaced pediatric supracondylar humerus fractures: Biomechanical analysis of percutaneous pinning techniques. J Pediatr Orthop 2002;22:440-3.
12. Wang X, Feng C, Wan S, Bian Z, Zhang J, Song M, et al. Biomechanical analysis of pinning configurations for a supracondylar humerus fracture with coronal medial obliquity. J Pediatr Orthop B 2012;21:495-8. doi: 10.1097/BPB.0b013e328355d01f.
13. Bloom T, Robertson C, Mahar AT, Newton P. Biomechanical analysis of supracondylar humerus fracture pinning for slightly malreduced fractures. J Pediatr Orthop 2008;28:766-72. doi: 10.1097/BPO.0b013e318186bdcd.
14. Silva M, Knutsen AR, Kalma JJ, Borkowski SL, Bernthal NM, Spencer HT, et al. Biomechanical testing of pin configurations in supracondylar humeral fractures: The effect of medial column comminution. J Orthop Trauma 2013;27:275-80. doi: 10.1097/BOT.0b013e31826fc05e.
15. Heffernan MJ, Lucak T, Igbokwe L, Yan J, Gargiulo D, Khadim M. The reverse oblique supracondylar humerus fracture: Description of a novel fracture pattern. J Pediatr Orthop 2020;40:e131-7. doi: 10.1097/BPO.0000000000001395.
16. Kang S, Kam M, Miraj F, Park SS. The prognostic value of the fracture level in the treatment of Gartland type III supracondylar humeral fracture in children. Bone Joint J 2015;97-B:134-40. doi: 10.1302/0301-620X.97B1.34492.
17. Kamara A, Ji X, Liu C, Liu T, Wang E. The most stable pinning configurations in transverse supracondylar humerus fracture fixation in children: A novel three-dimensional finite element analysis of a pediatric bone model. Injury 2021;52:1310-5. doi: 10.1016/j.injury.2021.01.012.
18. Lamdan R, Liebergall M, Gefen A, Symanovsky N, Peleg E. Pediatric supracondylar humerus fractures: Effect of bone-implant interface conditions on fracture stability. J Child Orthop 2013;7:565-9. doi: 10.1007/s11832-013-0533-4.
19. Bozoğlan M, Kumbaraci M, Özer A, Turgut A. Comparison of different fixation confi gurations in different types of high pediatric supracondylar humerus fractures: A finite element analysis. Acta Chir Orthop Traumatol Cech 2023;90:408-15.
20. Ji X, Kamara A, Wang E, Liu T, Shi L, Li L. A two-stage retrospective analysis to determine the effect of entry point on higher exit of proximal pins in lateral pinning of supracondylar humerus fracture in children. J Orthop Surg Res 2019;14:351. doi: 10.1186/s13018-019-1400-x.
21. Wang W, Li Q, Kamara A, Han Z, Liu T, Wang E. Analysis of the location and trajectory of the Kirschner wires in the fixation of extension-type supracondylar fracture of the humerus by 3D computational simulation. J Shoulder Elbow Surg 2022;31:1368-75. doi: 10.1016/j.jse.2021.12.048.
22. Hamdi A, Poitras P, Louati H, Dagenais S, Masquijo JJ, Kontio K. Biomechanical analysis of lateral pin placements for pediatric supracondylar humerus fractures. J Pediatr Orthop 2010;30:135-9. doi: 10.1097/BPO.0b013e3181cfcd14.
23. Pothong W, Phinyo P, Sirirungruangsarn Y, Nabudda K, Wongba N, Sarntipiphat C, et al. Biomechanical Analysis of Sagittal Plane Pin Placement Configurations for Pediatric Supracondylar Humerus Fractures. Appl Sci (Basel) 2021;11:3447.
24. Meng Y, Pak W, Guleyupoglu B, Koya B, Gayzik FS, Untaroiu CD. A finite element model of a six-year-old child for simulating pedestrian accidents. Accid Anal Prev 2017;98:206-13. doi: 10.1016/j.aap.2016.10.002.

25. Xu M, Qu W, Wang Y, Zhong L, Zhu Z, Li W, Zhao X, Wang J, Sun Y. Theoretical implications of periacetabular osteotomy in various dysplastic acetabular cartilage defects as determined by finite element analysis. Med Sci Monit 2016;22:5124-5130. doi: 10.12659/msm.902724.
26. Rancourt D, Shirazi-Adl A, Drouin G, Paiement G. Friction properties of the interface between porous-surfaced metals and tibial cancellous bone. J Biomed Mater Res 1990;24:1503-19. doi: 10.1002/jbm.820241107.
27. Eberle S, Gerber C, von Oldenburg G, Högel F, Augat P. A biomechanical evaluation of orthopaedic implants for hip fractures by finite element analysis and in-vitro tests. Proc Inst Mech Eng H 2010;224:1141-52. doi: 10.1243/09544119JEIM799.
28. Liu C, Kamara A, Liu T, Yan Y, Wang E. Mechanical stability study of three techniques used in the fixation of transverse and oblique metaphyseal-diaphyseal junction fractures of the distal humerus in children: A finite element analysis. J Orthop Surg Res 2020;15:34. doi: 10.1186/s13018-020-1564-4.
29. Schmucker A, Chen R, Vachhrajani S, Martinek M, Albert M. Radiation exposure in the treatment of pediatric supracondylar humerus fractures. Arch Orthop Trauma Surg 2020;140:449-55. doi: 10.1007/s00402-019-03251-2.
30. Gordon JE, Patton CM, Luhmann SJ, Bassett GS, Schoenecker PL. Fracture stability after pinning of displaced supracondylar distal humerus fractures in children. J Pediatr Orthop 2001;21:313-8.